PONTIFICIA UNIVERSIDAD CATÓLICA DEL PERÚ

FACULTAD DE CIENCIAS E INGENIERÍA

Study of models for the nominal power characterization of a photovoltaic generator and the power estimation of different photovoltaic technologies in Lima, Peru

Tesis para obtener el título profesional de LICENCIADO EN FÍSICA

AUTOR

Brando Xavier Calsi Silva

ASESOR

Prof. Dr. Jan Amaru Palomino Töfflinger

Lima, 1 de March de 2022

Agradecimientos

Quiero agradecer al Dr. Jan Amaru Palomino Töfflinger por el apoyo desde un inicio en mi interés en temas de energías renovables, mi introducción en tecnologías fotovoltaicas, por enseñarme sobre la física de las celdas, la asesoría en trabajos previos y motivación para poder seguir investigando. Dr. Juan de la Casa por su aporte de su vasta experiencia en las discusiones que me permitieron avanzar. Al grupo de Ciencias de los Materiales y Energías Renovables, mis compañeros y amigos. Mg. José Rubén Angulo y Mg. Luis Ángel Conde por su apoyo y asesoramiento en los proyectos y compañeros de viaje en los simposios. Apoyo financiero por CONCYTEC-PROCIENCIA mediante el proyecto con el contrato N° 124-2018-FONDECYT. Apoyo financiero del vicerrectorado para investigación de la Pontificia Universidad Católica del Perú (PUCP) (proyecto no. CAP-2019-3-0041/702). Igualmente, por el apoyo financiero mediante el Programa de Apoyo al Desarrollo de Tesis de Licenciatura (PADET). Colaboración con la compañía GERION INGENIERÍA por las facilidades y la disponibilidad del monitoreo del generador fotovoltaico. Finalmente, a mis padres y hermana por su ayuda incondicional a lo largo de mi carrera.

Abstract

This work investigates two main aspects related to photovoltaic: systems and module characterization and performance modeling.

The first part aims to characterize a PV generator located in Spain with a nominal power of 109.44 kW under standard test conditions according to the datasheet. An operational photovoltaic system's nominal power is a valid parameter for determining its current operational state. The applicability of a standard procedure to estimate the nominal power of an operating generator, proposed by Martínez-Moreno and based on Osterwald's model, is investigated. However, the standard procedure does not specify how to deal with experimental data when unexpected behavior impedes the nominal power estimation under operating conditions. During the 6-month study, the power-irradiance relation showed a hysteresis effect with varying amplitudes throughout the campaign. Adding a data filter that removes the non-linear part of the data proves necessary to estimate the nominal power, complementing Martinez-Moreno's procedure to enable the generators' characterization.

The second part contributes to closing a knowledge gap in the performance behavior and predictability of multiple PV technologies in Peru. The quality of two simple analytical models for estimating the outdoor performance of three different photovoltaic module technologies in Lima was investigated. Osterwald's and the Constant Fill Factor models were applied to estimate the maximum power delivered by an Aluminum Back Surface Field, a Heterojunction with Intrinsic Thin-layer, and an amorphous/microcrystalline thin-film tandem PV module. The results point that both models overestimate the expected power compared to the measured one. Implementing a correction factor adjusts the estimated maximum power by both models. This correction factor

allows us to estimate losses, calculate an adequate nominal power and minimize the estimated power error. The normalized root mean square error and mean bias error determine the implemented methodology's quality. The two crystalline silicon-based technologies present a similar behavior throughout the year. However, both differ considerably from the tandem one during different months, implying that the ambient variables have other seasonal impacts on their performance.

Contents

List of Figures

List of Tables

1 Introduction

1.1 General Introduction

The energy infrastructure of modern society is highly dependent on fossil fuels. The latter is nothing more than a form of solar energy that has been stored as chemical energy by photosynthesis processes and stored for millions of years in the form of gas, coal, and oil. Burning fossil fuels releases greenhouse gases such as carbon dioxide (CO_2). These gases released by human activity are stored in the oceans and atmosphere, warming them up and interfering with the water cycle, reducing snow and ice, rising sea levels, and climate change [1]. To address this issue, around 77 countries announced their commitment to a net reduction of zero carbon emissions by 2050. Due to this, they have to increase usage of renewable energies, such as wind, solar, biomass, hydroelectric, among others [2].

The annual solar energy incident on the earth's surface is around 10000 times more than the current global energy consumption in a year [3]. Photovoltaic (PV) technology takes incident solar energy and transforms it directly into another more useful form, electrical energy. There are currently various PV technologies; the most common on the market are crystalline Silicon, thin-film, and multi-junction [1,4]. 95% of the production share is represented by c-Si module technology [5]. In recent years, energy production has increased rapidly, where silicon-based modules make a large portion, Figure 1. The latter groups Multi-Si and Mono-Si technologies; Multi-Si modules are less efficient and cheaper compared to Mono-Si. Thin-film modules represent a small part of the annual energy production because they are less efficient, but the manufacturing process requires fewer resources [1,3].

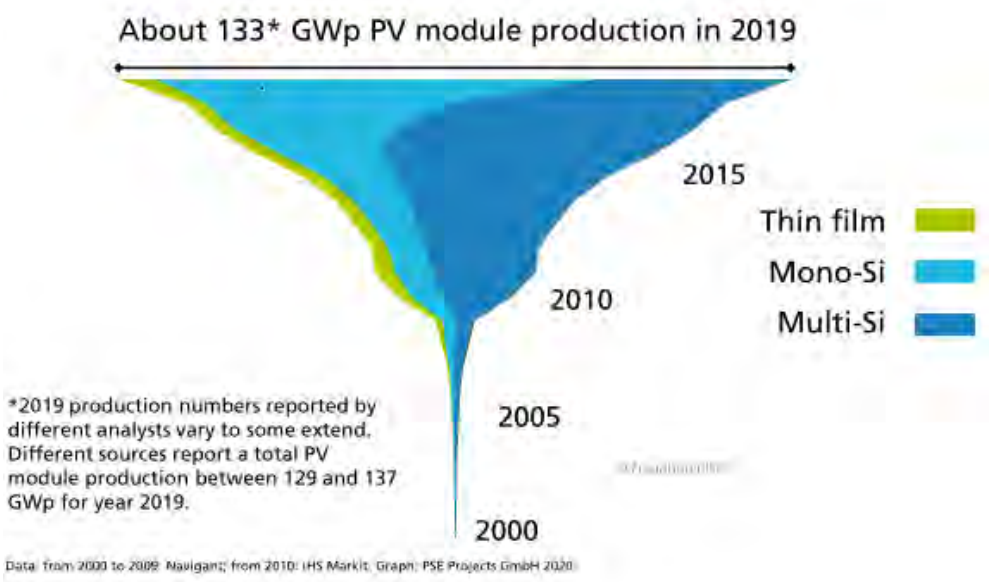

Figure 1. Annual world energy production by technology, taken from [5]

Peru comes into question in implementing PV technology because it has a diverse mix of coastline, jungle, and mountains that stretch across the country. The Peruvian Andes represents the largest concentration of high altitude peaks in the Americas that could prove to be viable locations for solar installations, considering that other parts of the world are taking initiatives to produce energy in a renewable way, and some installations in high altitudes with good performance [2]. Installations in the country's southern coastal area would result in high electrical energy potential; SOLARGIS [6] estimates a power potential at around 6 kWh/kW as a daily average, Figure 2. The latter refers to the energy (kWh) produced in one day for every thousand watts of nominal power installed (kW). This amount translates to about 2191 kWh/kW per year. The entire Peruvian coastline depicts a similar potential. By comparison, Peru's PV energy potential is more significant than most European countries; however, they have more PV systems installed [7]. The latter would exemplify Peru's PV power potential in the future if similar cumulative installations were to settle. There are currently seven PV plants operating in Peru, located in the southern coastal area, adding 280.48 MW and four in construction adding 576.46 MW resulting in a total of 856.94 MW [8–10].

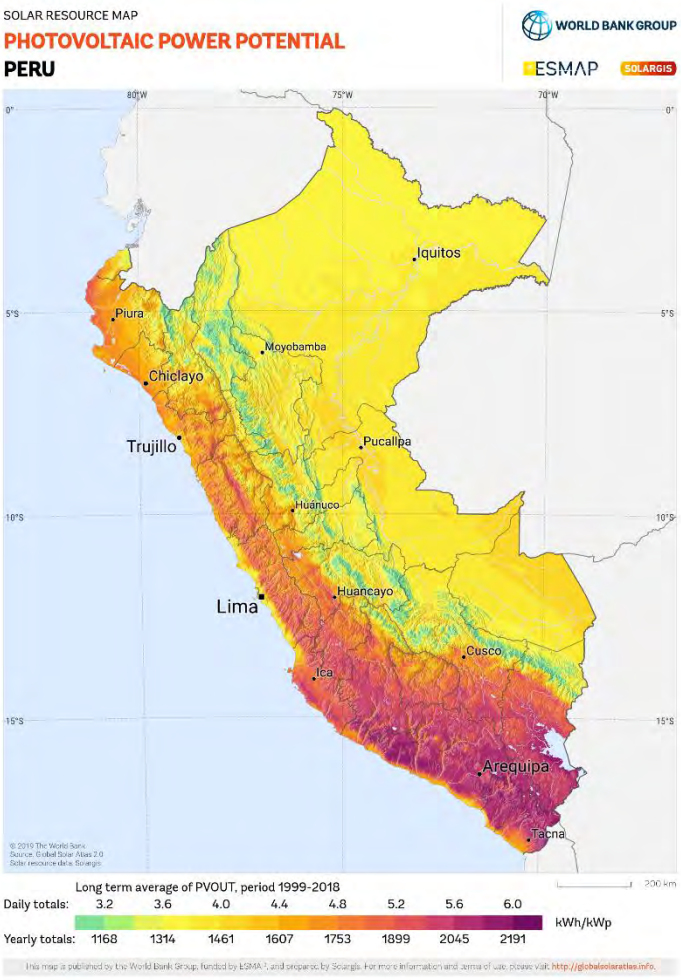

Figure 2. PV Power potential of Peru, taken from [6]

The increase in recent years of global PV installations has been primarily due to large-scale systems [11], which requires the assurance of their long-term operation to investors. For this purpose, international standards define the system's characteristic parameters when evaluating the PV generator status [12]. One of the main parameters is the nominal power of the system; this refers to the output power of the system at the maximum power point when subjected to the standard test conditions (STC) such as irradiance of 1000 W/m^2, AM 1.5 spectrum, and uniform module temperature of 25 °C, defined in IEC60904-3 [13]. These measurements require laboratory conditions applicable only on module level before their installation in the field. Reasonable doubts may arise on the total nominal power of the entire PV system after its installation, for instance, due to module mismatch and cable resistance losses. As time passes, the environment can cause degradation mechanisms such as initial

degradation due to UV light, elevated temperatures, hot spots, and shading, decreasing the PV system nominal power [14–18]. Incorrect choice of PV technology for a specific location may result in a fault design of a project due to ambient conditions, and thus performance is site-specific [14,17,19]. In this sense, it is important to estimate a PV system's main parameters in actual operating conditions [20], increasing the accuracy of the PV generator performance to ensure its correct operation within the manufacturer's assurance range.

Peru's growing demand for energy motivated the government to implement sustainable solutions, especially in rural areas with no connection to the national electrical grid. PV installations are currently the most used technology for rural electrifications projects [21–25]. Nevertheless, literature regarding the experimental quantification of PV yield and performance in Peru, even in Lima, is scarce due to limited studies for this region [21,22,26]. Absence knowledge of PV technologies performance can lead to technical risks and negative economic impacts in implementing PV projects [27]. Sadly, there is no public information on the detailed operation of the large PV systems already installed in the country because private companies maintain them. Further studies of the power and energy performance of various technologies in Peru may enable subsequent studies on their technical- and socio-economic performance, thus, enhancing the consciousness of PV's socio-economic potential among the population. Such consciousness must drive politicians towards new distributed generation regulations and incentives for PV generation, such as net metering and feed-in tariffs. Those protocols would benefit everyone and enable the integration of PV systems to the electrical grid or micro-grid on any scale (urban, commercial, industrial, and rural) [7]. Following the trend in Latin American countries, the Peru government approved in 2018 policies of autogeneration and distribution with net-metering and feed-in tariff [9,28].

For PV power estimation purposes, one may often find a trade-off between simplicity and accuracy in those models. In some cases, simplicity may be preferable, for instance, if

accuracy requires parameters that are not commonly available or use complex algorithms [19]. Studies have been done comparing the accuracy of different models and found that despite the simplicity of some, high accuracy of the estimated power can be achieved [19,29]. Therefore, studies are required to determine the PV performance estimation to determine the quality of models for predicting the outdoor PV power production for different technologies on the installation site.

1.2 Outline

This thesis is organized into six sections. Following this introduction, Section 2 provides the theoretical framework and definitions of the used parameters, the PV performance factors, and the utilized models. Section 3 describes the experimental details of two case studies. The first presents the configuration of the PV generator of 109.4 kW located in Granada, Spain. Similarly, the second subsection introduces the PV research laboratory and the setup for studying three PV technologies in Lima, Peru [30]. Section 4 illustrates the procedure followed for estimating the nominal power of a PV generator. Section 5 exhibits the methodology for studying three different PV technologies in single modules using two commonly used simple parametric models for power estimation [19]. Section 6 discusses the PV generator's estimated nominal power and analyses the three PV technologies' modeled power. Finally, Section 0 summarizes the conclusions and future work.

2 Theoretical Framework

This chapter introduces the basic concepts to understand the operation and dependence of the PV cell and the environmental factors that influence its behavior. The first part describes the fundamental structure of the cell and processes involved in the transformation of solar energy into electricity. From there, the factors that influence the performance of PV technology are briefly reviewed, such as irradiance, temperature, soiling, cell characteristics, among others. The last part presents the models used for estimating the output power.

2.1 Fundamentals of PV technology

The most widely used material in PV and from which the first successful solar cell was made is crystalline Silicon (c-Si) [1]. For this reason, the present work will explain the concepts of PV using c-Si. These concepts will give a basic understanding of how solar cells made of other materials work. The photovoltaic effect is the principle on which solar cells are based. This effect is closely related to the photoelectric effect, where electrons are emitted from a material when photons are absorbed. Similarly, the PV effect generates a potential difference in the union of two different materials in response to electromagnetic radiation [3]. When solar energy is converted directly to electricity using semiconductor materials, it is called the PV effect [1].

Silicon semiconductors behave as a conductor or insulator depending on an electric or magnetic field, radiation, temperature, among others. The semiconductor is characterized by having a conduction and valence band. The region that lies between the valence and conduction band is known as the bandgap, where the bandgap energy (E_G) is calculated as the energy difference between the minimum attainable conduction band energy (E_C) and the maximum attainable valence band energy (E_V), Figure 3. Photons with an energy equal to or greater than the E_G can be absorbed. The photon's absorption excites an electron (red circle) from the

valence band to the conduction band, leaving a vacuum in the valence band. This vacuum will behave like a particle with a positive elemental charge known as a hole (white circle) [1,3].

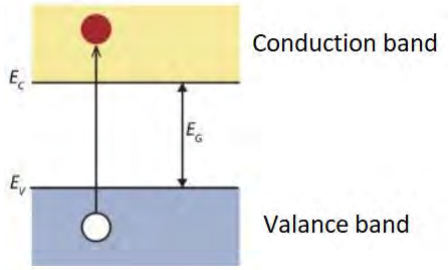

Figure 3. Basic energy band diagram of a semiconductor with electron-hole pair generation, red and white circle respectively [1]

A PV cell can be represented by the union of two membranes, where each of these has semi-permeable membranes that facilitate the collection of electrical energy. In solar cells based on c-Si, a membrane is composed of Silicon to which phosphorous impurities are incorporated. It is called n-type material because each phosphor provides a free electron, usually called donors. The second Silicon membrane contains Boron impurities, which provides a hole for each impurity called p-type material due to the hole's positive charge, calling them acceptors. The region between both membranes' junctions is the p-n junction, where an electric field is created due to the negative and positive charges corresponding to each membrane [1,3].

The PV effect can be divided into three basic processes: the generation of charge carriers due to photons absorption at the p-n junction, separation of the photogenerated charge carriers, and the collection of those charge carriers at the contacts. Once the electron-hole pair is generated, it would usually recombine in a conductor since there is no bandgap. In the insulator case, this bandgap energy is considerable, so the generation of the electron-hole pair requires a high amount of energy to excite one electron from the valance band. In the case of semiconductors, the photogenerated charge carriers that reach the contact can be collected through an external circuit. In this way, the electrons are only required to flow through the top

membrane, usually n-type material, and the holes through the lower membrane, p-type material, through electrical contacts. Once the electron is removed, it can work and be converted to electrical energy. After the electrons pass through the external circuit, they recombine with the holes near the metal interface and the lower membrane, p-type material [1,3].

2.2 Factors influencing the performance

PV technology's performance strongly depends on environmental factors such as irradiance, temperature, soiling, inclination, tilt angle, among others. To estimate PV output power, meteorological knowledge of the installation site is necessary [29]. As the current-voltage curve and technology or material of the PV cell, electrical characteristics must also be considered [18,31]. This section discusses these factors to understand the PV module's behavior in outdoor conditions.

2.2.1 Irradiance

Solar radiation is unpredictable and dependent on random phenomena; because of this, PV designs are based on statistical analysis from years of observations. The random nature results in an inevitable uncertainty for models and designs [29]. The amount of incident solar power, integration of radiation per wavelength, per unit area is known as irradiance. The PV cell produces electrical energy directly related to the irradiance available. The latter fluctuates along the year due to changes in the weather and air mass, solar beam's optical path length through the atmosphere, which affects the spectral distribution of incoming solar irradiance; due to this, the irradiance is site-dependent [3]. Additionally, the irradiance changes during the day because of variations in [18]:

- Sun's altitude,
- The angle between the horizontal plane and the sun,

- Azimuth
- The angle between the true north
- Projection of the sun rays to the horizontal plane

The incident solar irradiance on a surface consists of direct, diffused, and reflected components. The most significant fraction of the solar irradiation comes from the direct component; the diffused and the reflected components must be considered for the PV operation analysis [3]. It should be noted that the in-place irradiance, which depends on the inclination and tilt of the modules, absorbed by the modules is different from the global horizontal proportionated by various institutions [29]. The latter adds to the uncertainty of the models for modules, whether on a fixed or sun-tracking installation.

Additional considerations can be made from the irradiance effect in PV cells, such as optical losses due to crystal reflections for angles higher than 60° or spectral losses. The latter can be attributed to lower irradiation losses, which commonly occur at higher incident angles for fixed systems or a high amount of the diffuse component. The angular losses have been pointed as the main reason for high uncertainties for PV output power estimations [32]. For regions where the presence of clouds is predominant, the clouds' effect has to be considered in the irradiance analysis since it would result in the prevalence of the diffuse irradiance component [20]. The reflected component (or albedo) comes into consideration when working with bifacial modules, which transform the incoming irradiance on both sides of the PV module [33]. The produced electrical current is different on each wavelength of the solar spectrum of the solar radiation, usually called spectral response. The variation of the solar spectrum varies along the day and year, resulting in losses or gains on the electrical output of PV cells. Each technology has a different spectral response, i.e., thin-film modules are characterized by high spectral sensitivity resulting in losses of 3% in power production [29]. The electrical output of

a PV cell increases with solar irradiance. A positive linear relationship between the I_{SC} and the irradiance is expected due to the increase of absorbed light used to excite charge carriers that can be used to drive an electric circuit [34]. This relationship leads to an increased current and a slight increase in voltage, Figure 4 (a).

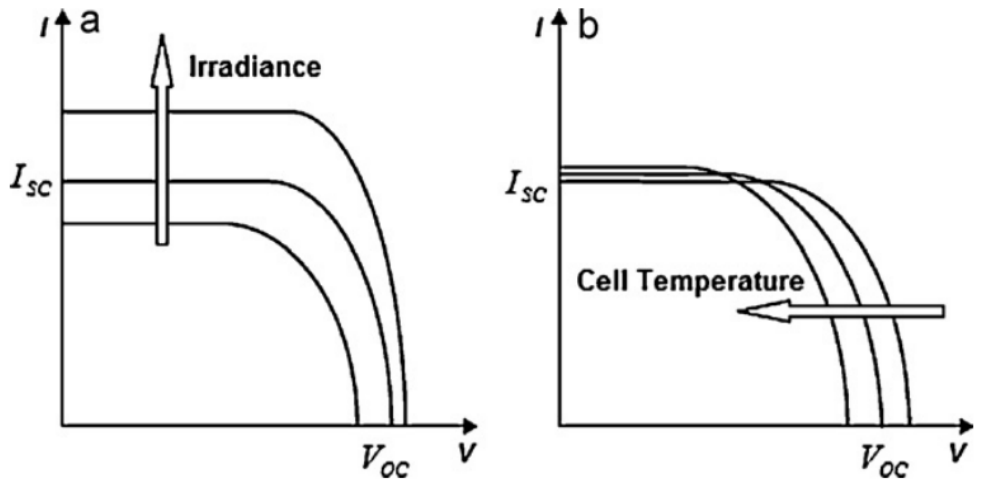

Figure 4. (a) Effect of increased irradiance and (b) cell temperature on I-V curve short-circuit current (I_{SC}) and open-circuit voltage (V_{OC}) [35].

2.2.2 Cell Temperature

The cell temperature (T_C) comes from the energy balance between solar irradiation, conduction, radiation, solar convection, and electricity production [29]. PV modules operation is affected mainly by the temperature caused by overheating due to solar radiation and high ambient temperature [36]. Increasing cell temperature shrinks the semiconductor's bandgap energy, allowing a more significant percentage of incident light to be absorbed because they have enough energy to excite charge carriers [1], Figure 4 (b). This increase of T_C on the PV panels affects the power output appreciably even in similar irradiance values [37]. Consequently, T_C is inversely proportional to the output power and efficiency. V_{OC} approximately decreases linearly with the rise in cell temperature [18].

The Nominal Operation Cell Temperature (NOCT) estimates the T_C, defined as the expected temperature when installed on an open structure of 45 ° of inclination submitted to an

irradiance of 800 W/m^2, 25 °C T_C, and 1 m/s wind speed, being at open circuit configuration [36]. The latter is defined in IEC 61215 (2005) for c-Si and IEC 61648 (2008) for modules based on thin-film technology [38]. The NOCT model implies that the heat transmission process is predominantly influenced by ambient temperature (T_a) conduction through the encapsulation material and not by convection from the wind. Due to the latter, the NOCT model could involve significant uncertainty for a non-stationary or windy environment [29]. Wind speed correction is considered second-order and practically impossible to predict; moreover, the importance of determining temperature is minimized when extrapolating in terms of the PV module's output electrical power [39]. The value of NOCT, constant value, is provided by the manufacturer, and module temperature is estimated using the following:

$$T_c = T_a + \frac{NOCT - 20\,°C}{800\,W/m^2} \cdot G \quad (1)$$

Tc is cell temperature, Ta stands for ambient temperature, NOCT is the nominal operating cell temperature, and G represents the in-plane irradiance.

There are temperature coefficients for electrical parameters such as short-circuit current (α), open-circuit voltage (β), power (γ), or form factor due to the thermal behavior of solar cells. These coefficients are commonly implemented on the PV power estimation and are inside a range for each technology [40]. Standard temperature coefficients for Si-based cells and modules are presented in Table 1.

Table 1. Typical Si solar cell temperature coefficients [40].

Type	α [ppm/°C]	- β [ppm/°C]	- γ [ppm/°C]
Si cells & modules	400-980	2400-4500	2600-5500

2.2.3 Soiling

Soiling can be differentiated by the uniform presence of dust or spotted dust such as bird droppings. Dust accumulated on the PV panel's surface can cause long-term sedimentation causing cell shading, thus obstructing incident light on cells. Soiling can be especially problematic in infrequent rainfall seasons or arid regions [18]. The deposition of dust over time and the loss of power depends on the environmental conditions and on-air pollution; consequently, it depends on the installation site [41]. In studying the effect of dust deposition on PV panels, size distribution and materials must be considered [42]. Additionally, the initial moments of dust deposition speed are much faster in the early stages after cleaning the front surface [18]. Dust accumulation is significant for angles of incidence between 40° and 80° [29]. A study of sand's influence from the Sahara on glass shows that sand plays an essential role in crystallization [43]. The latter actively changes the glass properties and accelerates its degradation, meaning a loss in power generated in a module under similar conditions. Adding the soiling effects could reduce annual production by 10%, but the initial state is at the observer's discretion [29]. Cleaning might remove soiling, but it comes with its challenges. Mechanical dust removal includes brushing, blowing, vibrating, and ultrasonic driving [14]. Lamont and El Chaar have summarized the options for system cleaning, each with its advantages and disadvantages [44]. For example, brushing methods might permanently damage the panel's surface, and blowing requires high maintenance and energy [14]. For the reasons presented above, dust deposition, sedimentation, cleaning, and its effect on glass degradation must be considered to evaluate a PV module's electrical behavior.

2.3 Photovoltaic power estimation methodologies

The electrical characterization of PV cells is made through the I-V curve, which is the fundamental information mechanism to extract its parameters later used in methodologies. The I-V curve electrical parameters determination is commonly performed in the dark or under illumination [29]. The former methodology is easily performed under stable conditions, such

as T_a, assuming the parameters do not change with illumination and represent outdoor behavior. The latter, under illumination, extracts the parameters with lower accuracy due to unstable conditions but is helpful for models involving irradiance and temperature [29]. The I-V curve is commonly used to extract the MPP, followed by the inverter's algorithm, and get the power at MPP (P_{MPP}), the most common parameter to identify and classify PV modules.

Manufacturers indicate other electrical parameters such as short-circuit current (I_{SC}) and open-circuit voltage (V_{OC}) at STC. The relevance of using such parameters is questioned due to lower annual performance, resulting in multiple methods to estimate the behavior closer to outdoor conditions [29]. It should be noted that most of the models found in the literature have been developed for c-Si, the most prominent in the market and well-known performance.

The models that estimate the maximum power can be classified into translation and numeric [45]. Conversely, the translation models consider each point of the I-V curve and treat current and voltage separately. Experimental measurements are made under working conditions to translate to a new I-V curve in desired conditions. Numerical models apply semiconductor physics knowledge and estimate the power at the MPP without using the entire I-V curve. The latter is calculated using analytical methods or numerical iterations to solve a PV cell's electrical model. The extent of different methodologies is explained in great detail in [19,29,46]. Analytical models estimate electrical parameters without iterations within an acceptable range of uncertainty. Numerical methods are criticized for ignoring the rest of the I-V curve and relying on the accuracy of the MPP trackers algorithms from the inverter. Additionally, estimated parameters may lack physical significance in some cases, settle in a manner by starting values for each parameter [29]. Two analytical models were selected for the current work, which in prior studies predicted the PV power and energy generation accurately despite their simplicity [29,47].

2.3.1 Osterwald model

The first is Osterwald's model. It is considered one of the simplest and is explained in detail in [34]:

$$P_{Ost} = P_M^* \frac{G_i}{G_i^*}[1 + \gamma(T_c - T_c^*)] \quad (2)$$

Where P_{Ost} is the predicted maximum power by the model, P_M^* is the nominal power or power delivered by the module at STC, G_i stands for in-plane irradiance, G_i^* is the irradiance at STC, and T_C^* is the cell temperature at STC. From the equation, it can be highlighted that the P_M^* should be constant over time as it represents a characteristic value of the system. However, there are factors that the model does not consider, such as losses due to degradation, dust effect, shadows, among others. Also, discrepancies with the model have been observed when systems with one or two-axis solar trackers are studied [48]

2.3.2 Constant Fill Factor model

The second is the Constant Fill Factor (FF_K) model. Which estimates the MPP assuming the fill factor (FF) remains constant through all operating conditions. Additionally, the I_{SC} and V_{OC} have a linear relation with the G_i and T_C, respectively [29,47]:

$$P_{FF_k} = I_{SC} V_{OC} FF^* \quad (3)$$

$$I_{SC} = I_{SC}^* \frac{G_i}{G_i^*} \quad (4)$$

$$V_{OC} = V_{OC}^*[1 + \beta(T_c - T_c^*)] \quad (5)$$

Where P_{FFk} is the predicted maximum power. Like Osterwald's model, the gains or losses that the PV module may experience are not considered, as described above. Additionally, each cell is assumed to be identical in its electrical behavior [19].

3 Experimental details

This chapter introduces both experiment setups, the PV generator Calerilla and the photovoltaic research laboratory. The first system comprises 576 polycrystalline PV panels located in Granada, Spain. The second consists of multiple PV technologies, of which three are considered for the present work and are located in Lima, Peru.

3.1 Photovoltaic generator Calerilla

The PV generator is connected to the grid in southern Spain (Latitude: 37.287, Longitude: -3.055), Figure 5. This generator has an annual global horizontal irradiance of 1880 kWh/m^2 and an average ambient temperature of 13.3 °C, which is advantageous in producing electrical energy since it has high irradiation and low temperature [49]. The generator consists of 32 strings parallel to 18 polycrystalline modules (pc-Si) in series-connected per string. Additionally, the manufacturer's sheet nominal power is 109.44 kW, but with a nominal power of 100 kW from the inverter. Multiple works of members of the "Universidad de Jaén" are based on this generator [50–53] and were shared for further analysis from GERION INGENIERIA.

Figure 5. PV generator located in Granada, Spain [50]

The experimental campaign was carried out from the end of March to September 2018, avoiding the days where there were problems or maintenance of the generator, leaving 163 days for further analysis. Two calibrated PV modules with identical characteristics and

technology as the working modules measured ambient conditions. One of the modules was set on open-circuit (OC) to measure module temperature, and the other one in a short-circuit (SC) to quantify incident in-plane irradiance, respectively. It is assumed that the module temperature and irradiance represent the working conditions of the rest of the module's generator. The direct-current (DC) measurements were carried out at the inverter's input, using a programmable industrial sensor from the manufacturer Circutor, model DH96-CPM, and shunt resistor 500A - 150 mV (class 0.5). Likewise, the alternating-current power (P_{AC}) was monitored with a high-end wattmeter, Yokogawa brand, model WT1600S. A commercial Graphtec data acquisition system (midi LOGGER GL220 model) was used in the data collection and environmental parameters, saving the data every 30 seconds for the study period.

3.1.1 Clear day selection

Following the procedure suggested by Martinez-Moreno [54], a filtering procedure was developed to select only sunny days and a smooth curve of power vs. time during the entire day. The latter is to avoid shading in either the generator or irradiance module and sunny for measurements in high irradiances (more than 800 W/m^2) as required by the Osterwald model. First, days with problems in the recording process were filtered out, such as maintenance or disconnection. Secondly, employing a sinusoidal regression of the recorded P_{DC} was applied using Python, equation (6). The P_{DC} was used instead of G_i to avoid shade on the module that measures it.

$$F(x) = A\,sin(b.x), \;\; 0 < x < m \tag{6}$$

Where m stands for the number of the day datasets, $F_{(X)}$ represents the normalized P_{DC}. Ideally, the amplitude (A) is one since the P_{DC} is normalized, and b is $2\pi/2m$, which represents the period of the sinusoidal function. With the estimated a and b, the difference between the

normalized and adjusted P_{DC} was measured using RMSE. Experimentally a limit of 5% was established to select clear-sky days.

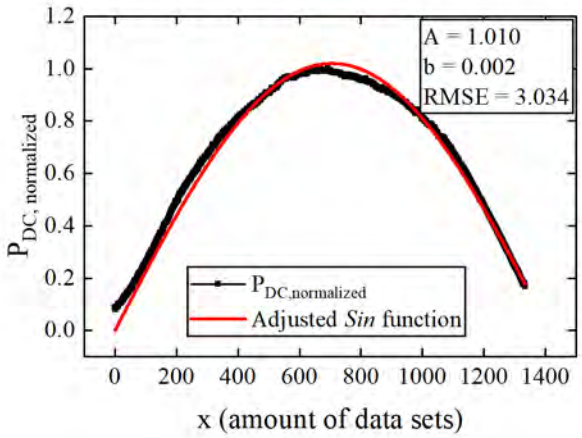

Figure 6. Sinusoidal adjustment function for identifying clear days

Figure 7 presents the different days encounter in the selection process. Smooth continuous datasets characterize sunny days (black dots). Cloudy days with peaks, higher values than the rest, along the day (red dots). Incomplete days where a small number of datasets were recorded with absent measurements along the day (blue dots). It was determined that there were 27 sunny, 122 cloudy, and 4 days with incomplete data.

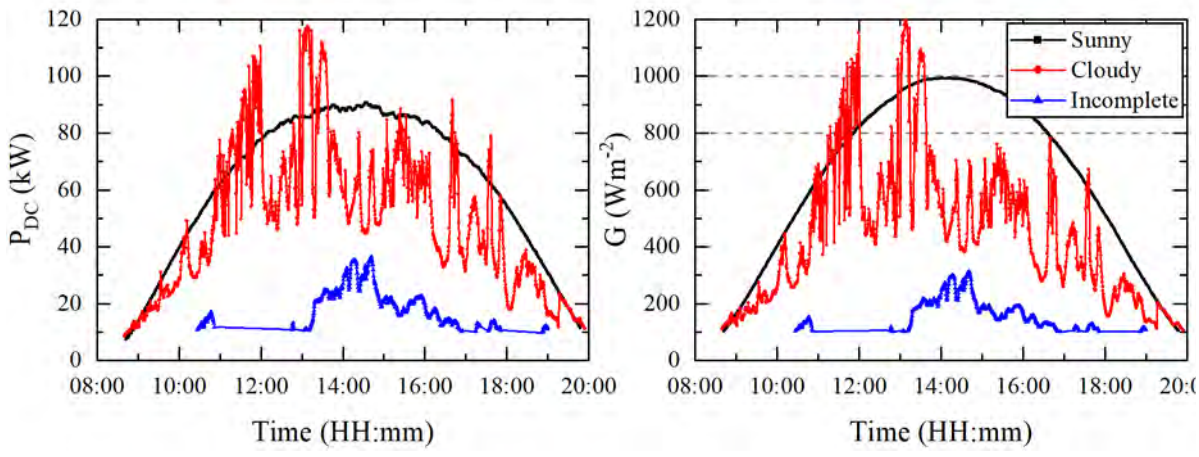

Figure 7. (a) Power and (b) and Irradiance examples for each day selections

3.2 Photovoltaic Research Laboratory

The Photovoltaic Research Laboratory is located in the Physics Section of the "Pontificia Universidad Católica del Perú" (PUCP) (12°4'S, 77°4'W) in Lima. Figure 8 shows the modules

under study in a structure with a tilt angle of 20° facing north. The I-V tracer is measured with two Keysight 34465A multimeters based on a capacitive load. The maximum power is extracted from each I-V curve. A tilted pyranometer EKO MS-80 measured the irradiance at the plane-of-array. Two class B PT100 pasted at the backside of each module were used to measure the module temperature. The whole laboratory is described in greater detail in [30,55]; it was developed based on the system described in [56]. The irradiance and module temperature were instantaneously measured at the IV curve trace's beginning and end. The electrical and meteorological datasets were recorded every 5 minutes for each PV module.

Figure 8. Photovoltaic Research Laboratory located in Lima, Peru

The experimental campaign for this thesis was based on three silicon-based PV module technologies: p-type polycrystalline Aluminum-Black Surface Field (Al-BSF), n-type monocrystalline Heterojunction with Intrinsic Thin-layer (HIT), and amorphous/microcrystalline (a-Si/µc-Si) thin-film Tandem.

3.2.1 Calibration procedure

The outdoor calibration procedure was conducted to contrast the experimental results and estimate the manufacturer's laboratory's electrical parameters, corresponding to the local conditions. Due to the overestimation of the power from both models, a correction factor (k)

was implemented. The latter was used to estimate each panel's calibrated characteristic electrical parameters after their first three months of installation (March to May 2019) in the Photovoltaic Research Laboratory [55]. Table 2 shows the characteristic electrical parameters at STC as given by the manufacturer. It also shows the respective calibrated values.

Table 2. Characteristic electrical parameters in STC of the PV modules and their calibrated values, taken from [55].

Technology	Electrical parameter	Datasheet	Calibrated
Al-BSF	$P_M^*\ (W)$	270	269.2
	$I_{SC}^*\ (A)$	9.32	9.45
	$V_{OC}^*\ (V)$	37.9	37.2
	FF^*	0.76	0.77
HIT	$P_M^*\ (W)$	330	324.6
	$I_{SC}^*\ (A)$	6.07	6.05
	$V_{OC}^*\ (V)$	69.7	70.4
	FF^*	0.78	0.76
a-Si/µc-Si Tandem	$P_M^*\ (W)$	128	127.9
	$I_{SC}^*\ (A)$	3.45	3.32
	$V_{OC}^*\ (V)$	59.8	59.1
	FF^*	0.62	0.65

Data sets of the I-V curve, irradiance, and module temperature, were collected during one year of monitoring, from June 2019 to May 2020. Each module was cleaned weekly to minimize soiling effects.

3.2.2 Filtering process

An effort was made to maximize our monitoring data quality to detect and remove erroneous or inconsistent measurements from the analysis. The ambient measurements were filtered first to ensure a proper relation to the module's electrical response.

3.2.2.1 Irradiance filtering

To ensure a stable solar irradiance during the I-V tracing process. Data sets with a difference in incident in-plane irradiance δG, in the same plane as the modules, over 4% were filtered out in this manner [57]. This limit was experimentally selected from the thermopile

pyranometer responsitivity expanded uncertainty of around 5% with a 95% confidence level [58].

$$\delta G = \frac{2 \times |G_{start} - G_{end}|}{G_{start} + G_{end}} \quad (7)$$

G_{start} and G_{end} stand for irradiance measurements at the start and end of the I-V tracing, respectively. It was assumed that G_i remained constant, withing the pyranometer expanded uncertainty, during the I-V curve measurement when δG was small.

3.2.2.2 Module temperature filtering

The measured module temperature was compared to the estimated module temperature using the Nominal Operation Cell Temperature (NOCT), equation (1). Differences (δT) beyond that value were filtered out. A limit of 50% was set experimentally, differences beyond the threshold were filtered out.

$$\delta T = \frac{|T_{measured} - T_{modelled}|}{T_{modelled}} \times 100\% < 50\% \quad (8)$$

$T_{measured}$ stands for the measured module temperature. The panel has two points where the temperature is measured, so the mean was only the representative value when both values satisfy the condition set above. If one of the points were filtered out, the other was taken as the representative value. When both measurements did not comply with the threshold, the entire dataset was dropped since the models needed cell temperature to estimate the output power.

3.2.2.3 Current-Voltage curve filtering

After validating the irradiance and temperature measurements, the I-V curves passed a filtering algorithm to avoid erroneous measurements that would lead to erroneous electrical parameter estimation, for instance, due to shading on the panel. For this purpose, steps were established to filter systematic failures observed during the first year.

The first step is to discard data that correspond to the pre-charge of the capacitor. A negative voltage is initially applied to ensure the voltage passes through zero to extract the I_{SC} [30]. In Figure 9 (a), there is a drop from the initial positive voltage (red dots) followed by a constant increase (continuous black dots) from negative voltage passing by 0 V until it reaches its maximum value, V_{OC}. In this sense, the filter identifies the minimum voltage's instant and eliminates the datasets previous to that moment (red dots). Additionally, negative voltage and current values were eliminated (blue dots). The measurements filtered in each step are also visualized in Figure 9 (b) of current measurements, where measurements corresponding to the pre-charge are filtered out. Complementary, Figure 9 (c) shows the filtered data in the I-V curve. Here, the filtered data points, red dots, from the pre-charge accumulate near the V_{OC} are hidden, but some appear near this point due to the jump from the V_{OC} to negative voltages, Figure 9 (c).

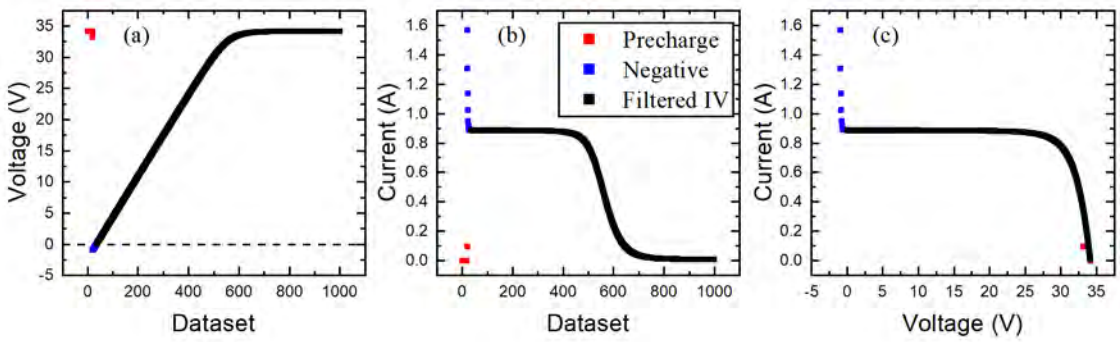

Figure 9. Identification of the (a) pre-charge and (b) negative values of the (c) I-V measurement

The second step is to identify systematic failures and filter the erroneous portion of the I-V curve. In Figure 10, erroneous measurements represented as red dots are present after the I-V curve trace is concluded when the V_{OC} is reached. In the last datasets, the current varies while the voltage is maintained constant. Similarly, in Figure 11, the voltage varies while the current stays at the minimum value, near 0 (red dots). The minimum current and maximum voltage instants were searched to filter the extended portion of the I-V measurement. The first

event is selected to filter out the rest of the measurements; e.g., if the minimum current is reached before the maximum voltage, then the measurements past that minimum current are filtered out. Additionally, this filter eliminates redundant measurements after completing the I-V tracing.

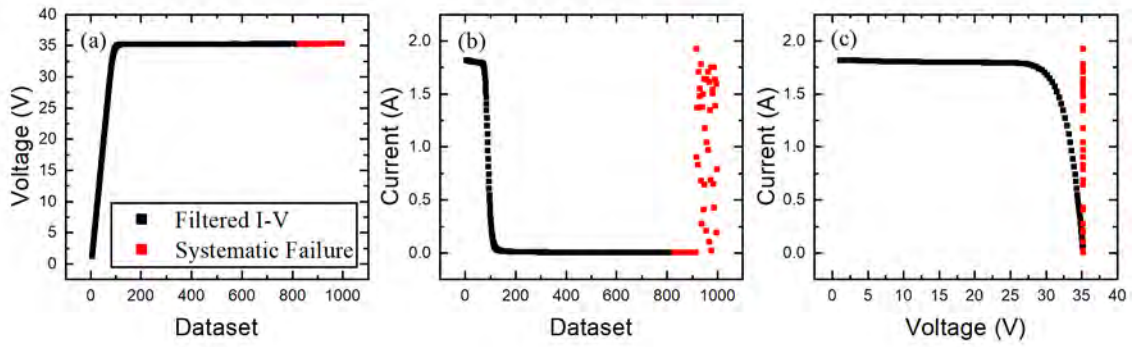

Figure 10. Variable current identification on synchronization discharge time failure. Datasets filtered by after achieved maximum voltage, (a) Voltage vs. Dataset, (b) Current versus Dataset, and (c) Voltage versus Current

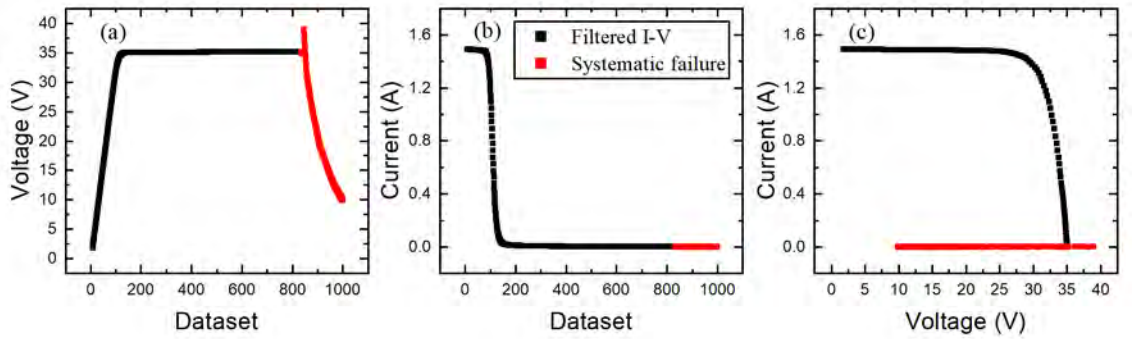

Figure 11. Variable voltage identification on synchronization discharge time failure. Datasets filtered by after achieved minimum current, (a) Voltage vs. Dataset, (b) Current versus Dataset, and (c) Current versus Voltage

A significant unknown step in the voltage and current is present in the middle of the measurement, where the maximum power point is located (Figure 12). A filter was implemented to identify such cases: It calculates the difference for each step of the I-V curve measurement and applies an experimental maximum step limit of 1.5 V and 0.1 A for the voltage and current, respectively. When one of the limits is surpassed, the I-V curve is not considered for the analysis.

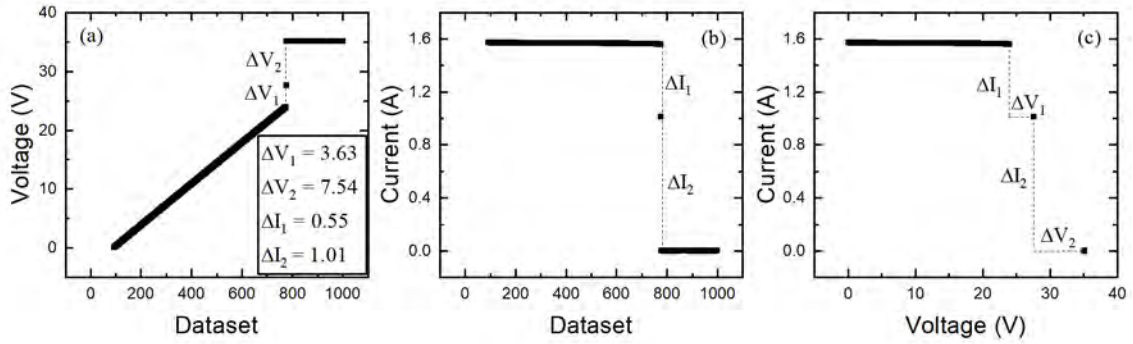

Figure 12. Low step homogeneity along with the I-V curve measurement. Difference of voltage and current between each step (a) Voltage versus Dataset, (b) Current versus Current, and (c) Current versus Voltage.

Additionally, to identify other systematic failures, the expected I_{SC} and V_{OC} values were calculated using Equations (5) and (9), respectively. A filter discarded I-V curves with relative differences between the measured and the computed values exceeding 30% and 15% for the I_{SC} and V_{OC}, respectively.

$$I_{SC} = I_{SC}^{*}\frac{G_i}{G_i^{*}}\left(1 + \alpha(T_c - T_c^{*})\right) \tag{9}$$

Another filtering process enables the detection of I-V curves affected by the shading of the panels. In Figure 13, a linear regression (blue line) was performed with the data sets with output power less than 80% of the maximum power (red dots). The normalized root mean square error ($NRMSE_{IV}$), defined in equation (10), was calculated, and a limit of 0.006 was established for the Al-BSF technology. In Table 3, the limits of $NRMSE_{IV}$ for detecting the shading of the modules are presented. This last value was determined experimentally in September due to a high number of I-V curves where the shading effect was observed. Its behavior was corroborated in the following months.

$$NRMSE_{IV} = \sqrt{\frac{1}{N}\sum_{i=1}^{N}\left(\frac{I_{modelled}(V)_i - I_{measured}(V)_i}{I_{SC,measured}}\right)^2} \tag{10}$$

Table 3. Values of $NRMSE_{IV}$ set to detect the shading of the module for the different technologies

Technology	$NRMSE_{IV}$
Al-BSF	0.006
HIT	0.008
a-Si/µc-Si Tandem	0.01

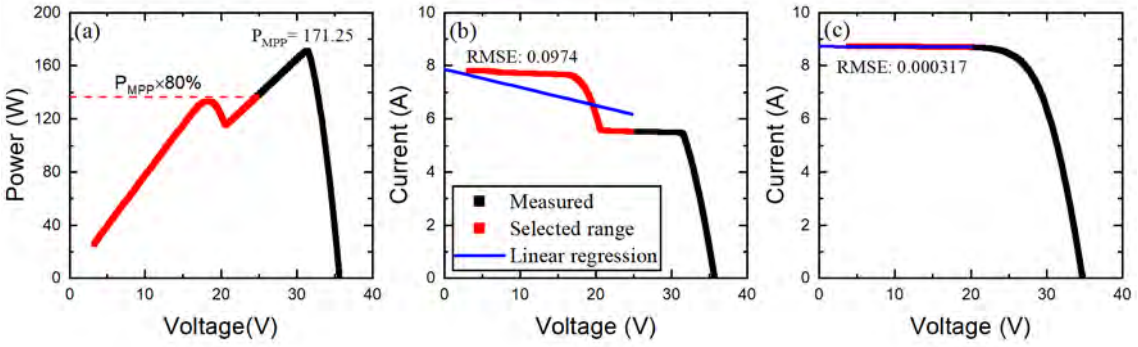

Figure 13. (a) The range for shade identification, (b) linear regression, $NRMSE_{IV}$, and (c) non-shaded curve with similar ambient conditions

Following the filtering steps described above, 121 000 measurements were processed, resulting in a drop of 10 %, with about 109 000 data sets remaining. The latter were considered high quality and used for further analysis in the current work. The before and after measurement amounts of the filtering procedure for each technology are presented in Figure 14. The filtering procedure appears to drop more datasets for the Tandem technology than the other technologies. The latter is possible due to unsuitable modeling of the expected I_{SC} described above, limited by the current of the lesser of the two sub-cell photogenerated currents [59], which may result in differences more significant than the established 15 %, mainly at irradiances lower than 80 W/m^2.

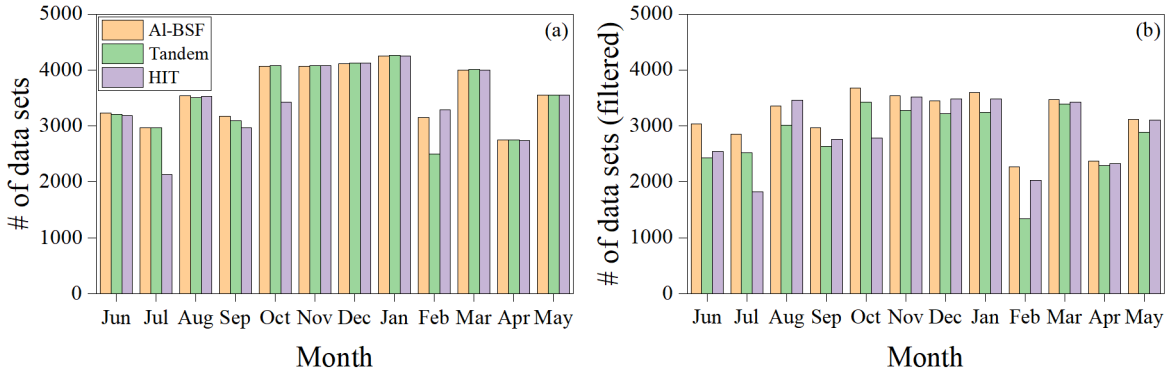

Figure 14. Amount of recorded data sets (a) before and (b) after the filtering procedure for each technology (from June 2019 to May 2020).

Figure 15 depicts the classification of local ambient conditions by each season. Spring: September – December, Summer: December - March, Fall: March - June, Winter: June - September. The irradiance and module temperature steps were defined as 50 W/m^2 and 5 °C, respectively. Each box represents the number of measurements normalized by one year, shown in percentage by the color scale. The irradiance distribution differs for each season, where high irradiances (from 800 to 1000 W/m^2) appear noticeably in the summer season. Nonetheless, a considerable portion is taken at low irradiances (from 0 to 300 W/m^2) throughout the year, especially during winter. In Lima, cloud presence is predominant during winter, spring, and autumn [60]. Note that STC represented by the black dot was never met; this emphasizes the need to investigate the performance of PV technologies under Lima's climatic conditions.

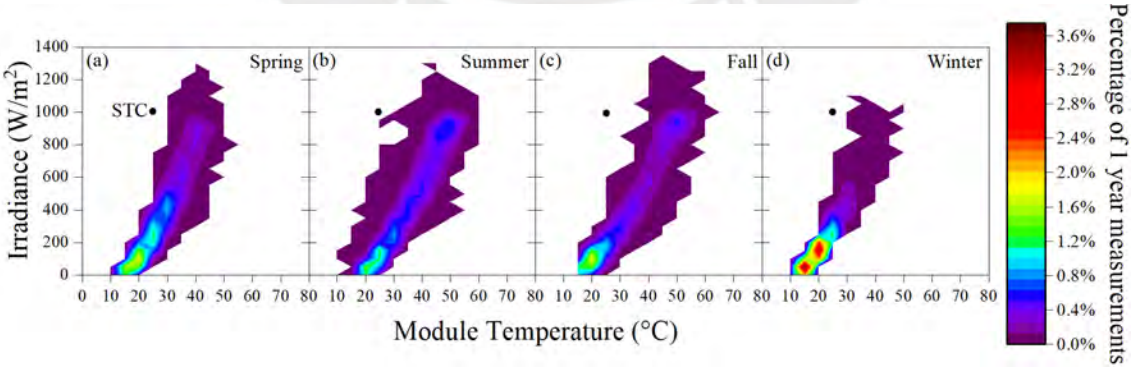

Figure 15. Percentage measurements by irradiance and module temperature for (a) Spring, (b) Summer, (c) Fall, and (d) Winter.

4 Procedure for calculating the nominal power of a photovoltaic generator

The present chapter presents the procedure to estimate the nominal power for the photovoltaic generator Calerilla in Spain. The methodology suggested by Martínez-Moreno was followed [54], based on Osterwald's equation (2).

4.1 Martinez-Moreno procedure

The procedure suggested for quality assurance is implemented to select clear days and previous filtering of anomalies, such as inverter saturation and shading. It is based on Osterwald's model, equation (2). The latter is used to estimate the nominal power implementing the correction of the P_{DC} values to 25 °C to minimize the module temperature power loss:

$$P_{T\to 25}^{DC} = \frac{P_{DC}}{1 + \gamma\,(T_M - 25)} \tag{11}$$

Data of high irradiance was used (between 800 and 1000 W/m^2) such that the non-linear behavior of corrected temperature power ($P_{T\to 25}^{DC}$) at low irradiances is avoided. As Martínez-Moreno points out in his work, the procedure assumes that the inverter perfectly follows the MPP and that the error of the temperature distribution along the generator has a Gaussian or normal distribution. Additionally, the reference modules used to measure module temperature and in-plane irradiance were located in a representative place (between the edge and the center at a medium height) [54]. However, when carrying out this procedure, a difference was observed between the $P_{T\to 25}^{DC}$ before and after the maximum corrected power, see Figure 16 (b). This effect is usually called hysteresis in the literature [48]. In this circumstance, it was considered relevant to clarify the data filtering method for correct adjustment and estimation of the system's nominal power.

4.2 Hysteresis

The hysteresis effects refer to the phenomenon where output values depend on the inputs' directional sequence application. The latter is mentioned in IEC 60751 [61] applied to the resistance thermometer PT100 and defined in IEC 61298-1 [62].

In the process of the P_M^* estimation, the relation of $P_{T\to25}^{DC}$ with G is used, which represents the complementary portion of the linearization of Osterwald's equation [54]:

$$P_{Ost} = P_M^* \frac{G_i}{G_i^*}[1+\gamma(T_c - T_c^*)] \rightarrow \frac{P_{Ost}}{1+\gamma(T_c - T_c^*)} = P_M^* \frac{G_i}{G_i^*} \rightarrow P_{T\to25}^{DC} = P_M^* \frac{G}{G^*} \quad (12)$$

For comparison, the P_M^* estimation was evaluated for three groups on the same day. The first, called linear, corresponds to the morning measurements till the maximum $P_{T\to25}^{DC}$. The measurements after the latter point correspond to the second group, which is called non-linear. The full-day group stands for the entire day's measurements, as a regular study would be conducted if the hysteresis effect was not present. Figure 16 shows the hysteresis effect for a particular day, June 21st of 2018, with the groups presented above. The sequence of the measurements is signposted with arrows and the procedure results for the particular day. Notice that the difference in power is better appreciated in low irradiances, lower than 800 W/m^2.

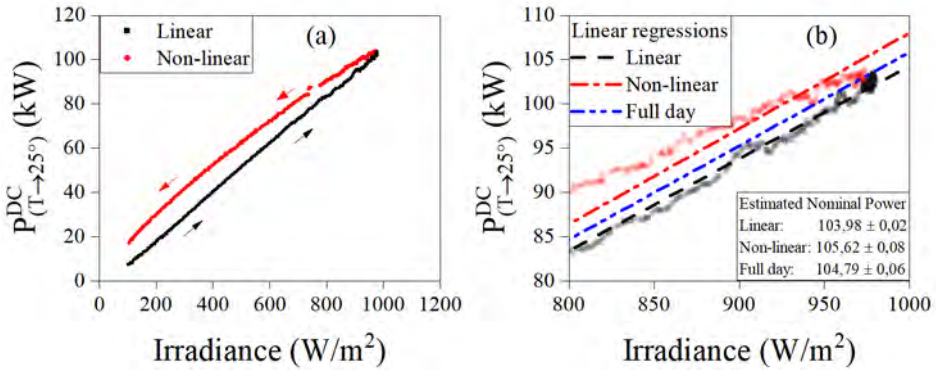

Figure 16. Corrected power ($P_{T\to25}^{DC}$) versus irradiance (G) as of June 21st, 2018, (a) data group selection and (b) linear regression of each group for the P_M^* estimation.

5 Monitoring versus power's estimation of three different PV technologies

In this section, the first year of operation of the Photovoltaic Research Laboratory of the Physics Section at the PUCP is presented alongside the analysis of three different PV technologies' nominal parameters using two analytical models for power estimation.

5.1 Effective nominal parameters

For each model, the estimated power was calculated using the calibrated parameters in Table 2 with the measured in-plane irradiance (G_i) and cell temperature (T_C) values. The measured power was obtained at each I-V curve's maximum power point (Pmpp). Exemplarily, Figure 17 displays the linear relation between the estimated power and the HIT module measured P_{MPP} using both models, Osterwald's ($P_{Osterwald}$) and Constant Fill Factor (P_{FFk}). Here, the data for the entire month of September 2019 is analyzed. Linear regression was used to correlate the estimated and measured power values. For both cases, the linear regression slope is slightly larger than 1: a = 1.052 and 1.051 for the Osterwald and the FFk model, respectively, indicating that both models overestimate the power by about 5% for the HIT module for this particular month.

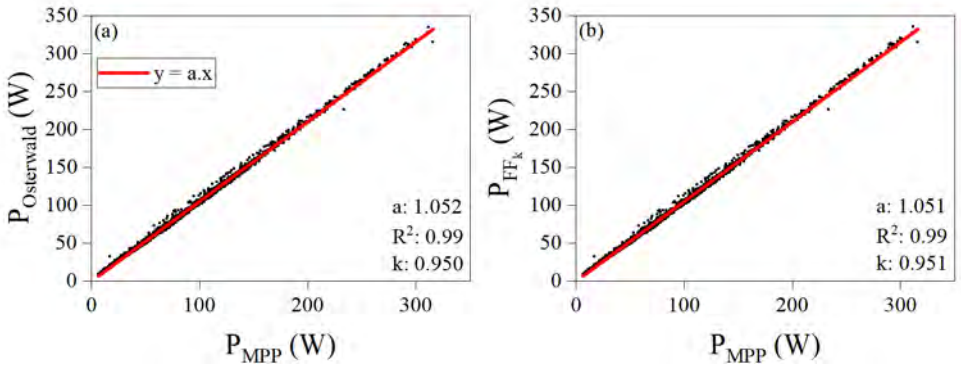

Figure 17. Estimated vs. Measured Power by (a) Osterwald and (b) constant fill factor (FF_k) model for the HIT module in September 2019.

A correction factor (k) was introduced to correct the estimated power. For each lapse of time (month and year), a k is established, this parameter represents estimated power adjustment:

$$P_{Ti} = P_{Oi} \cdot k^{-1}, with\ k = a^{-1}. \tag{13}$$

Here P_{Oi} represents the maximum instantaneous observed power, and P_{Ti} is the estimated power using Osterwald's or FF_K model. Values of k higher than one represent underestimation, while values lower than one stand for an overestimation, and equal to one indicates a correct estimation of the measured power:

$$k \begin{cases} > 1, & understimation \\ = 1, & correct\ estimation \\ < 1, & overstimation \end{cases} \tag{14}$$

Furthermore, given each model's correction factor, a correction of the nominal values can be suggested. In this manner, we propose to define the effective nominal parameters as:

$$P^*_{M,eff} = P^*_M \cdot k_{Osterwald} \tag{15}$$

$$FF^*_{eff} = FF^* \cdot k_{FF_k} \tag{16}$$

Where $k_{Osterwald}$ and k_{FFk} represent the correction factor for the Osterwald and the FF_K model, respectively, the effective nominal parameters represent the value of the characteristic electrical parameters installed outdoors in a specific place. For instance, in Figure 17, the results for September 2019 are 0.95 and 0.951 for $k_{Oserwald}$ and k_{FFk}, respectively. $P_M{}^*{}_{eff}$ stands for the effective nominal power, and $FF^*{}_{eff}$ for the effective nominal fill factor. By replacing $P_M{}^*$ with $P_M{}^*{}_{eff}$ in equation (2) and FF^* with $FF^*{}_{eff}$ in equation (3), we can obtain the "corrected" modeled power.

5.2 Statistics definitions

Two statistical metrics were applied to evaluate the quality of the methodology above. The Normalized Root Mean Square Error (NRMSE) provides information on the predicted

power dispersion concerning the measured one. Whereas the Normalized Mean Bias Error (NMBE) pictures the deviation or trend of the modeled values:

$$NRMSE = RMSE \cdot [\,\overline{P_O}\,]_{year}^{-1} \cdot 100\% = \left[n^{-1}\sum_{i=1}^{n}|P_{Ti} - P_{Oi}|^2\right]^{1/2} [\,\overline{P_O}\,]_{year}^{-1} \cdot 100\% \quad (17)$$

$$NMBE = MBE \cdot [\,\overline{P_O}\,]_{year}^{-1} \cdot 100\% = \left[n^{-1}\sum_{i=1}^{n}(P_{Ti} - P_{Oi})\right] [\,\overline{P_O}\,]_{year}^{-1} \cdot 100\% \quad (18)$$

P_T and P_O represent the modeled and measured power, respectively; n stands for the number of values considered during the period (month or year). $[\,\overline{P_O}\,]_{year}$ is the yearly average measured maximum power. These definitions of NRMSE and NMBE $[\overline{P_O}\,]_{year}$ differ from the definition used in other works [17,19,29]. In this case, the normalization was made with each technology's average power over the year ($[\,\overline{P_O}\,]_{year}$). The latter enables us to compare the NRMSE and NMBE values between months for the three technologies and the methodology [63]. Furthermore, it should be noted that the purpose of applying the correction factor k is to minimize the NMBE.

6 Results

6.1 PV generator's nominal power

The information gathered over seven months passed several filters to estimate the PV generator's nominal power. Martinez-Moreno suggests selecting sunny days to avoid low electrical output due to the shading of modules [54]. Osterwald's equation linearizes the relationship between irradiance and power by normalizing the cell's temperature (Equation 12). However, the hysteresis effect was observed. The daily nominal power estimation was carried out using three different data groups to analyze whether this behavior was present throughout the study period and clarify the procedure of Martinez-Moreno.

Figure 18 shows the daily P_M^* estimation using each group: linear, non-linear, and full-day. The linear's daily estimated nominal power is lower than the non-linear part. The latter exhibits the degree of the hysteresis effect on the experimental campaign, i.e., higher estimation on the first three months while decreasing in the following months. While the P_M^* values using the linear group are more stable during the experimental campaign and avoid an unknown factor. The full-day is not recommended because it shifts the estimation and misleads the evaluation of the generator's state. Due to the above, P_M^* estimation should consider the linear group to avoid abnormal behavior. The consideration of the non-linear part would result in an incorrect estimation since the irradiance and power relationship would not follow the expected response. Therefore, the hysteresis filtering process for high irradiances is relevant for the correct P_M^* estimation if the effect of hysteresis is present on a PV generator under study.

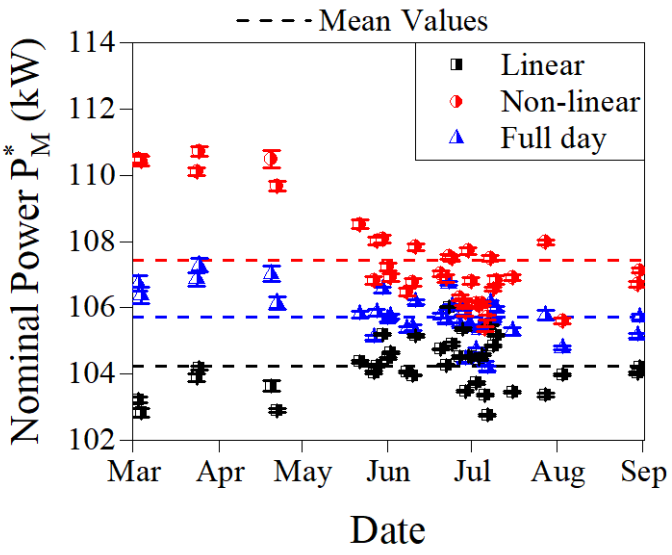

Figure 18. Daily Nominal Power estimation for each group: linear, non-linear, and full day.

6.1.1 Nominal Power Estimation

An empirical methodology allows the identification of anomalies in the operation of PV systems. The full-day group nominal power's average result is 105.71 kW, Figure 18. If we consider only the linear part of the data, we have a value of 104.24 kW and 107.43 kW for the non-linear part, respectively. Furthermore, the daily values of the non-linear part have a higher dispersion that also indicates a variance of the hysteresis, leading to higher values from March to May and lower ones from June to September. In contrast, the daily values considering only the linear part have lower dispersion and remain relatively constant throughout the six months. Table 4 collects the average estimated nominal power for each group and their errors concerning the one found in the datasheet of 109.44 kW. Within the estimated P_M^*, one observes that the non-linear part has the highest average or lowest error concerning the P_M^* from the manufacturer sheet. The error alone is not enough to have the whole picture since the difference could be related to experimental losses and deterioration. The linear part presents a lower standard deviation, indicating that this group is more in line with the Martinez procedure and, therefore, with the extensively studied Osterwald's model, which describes the expected behavior of the solar cell. The linear group's nominal power was considered the 'true' nominal

power since Osterwald's equation predicts a linear behavior. The hysteresis effect was later discussed. The most likely origin was spatial inhomogeneities of module temperature and plane-of-array irradiance, the latter from PV strings misalignments [64].

Table 4. Average, standard deviation, and difference of daily estimated nominal power.

Data set labels	P_M^* (kW)	Standard deviation	Difference (%)
Linear	104,24	0,05	4,71
Non-Linear	107,43	0,11	1,84
Complete	105,71	0,11	3,41

6.2 Analysis of the expected power of three different PV technologies

6.2.1 Correction Factor

Following the mentioned procedure in Section 5.1, the measured and modeled values were compared each month. The corresponding correction factor (k) was calculated to minimize the expected and measured power difference. In Figure 19, the monthly and the yearly k for the three PV technologies. For the monthly values, only data from the respective month was evaluated, whereas, for the annual values, the recordings of 12 months were analyzed.

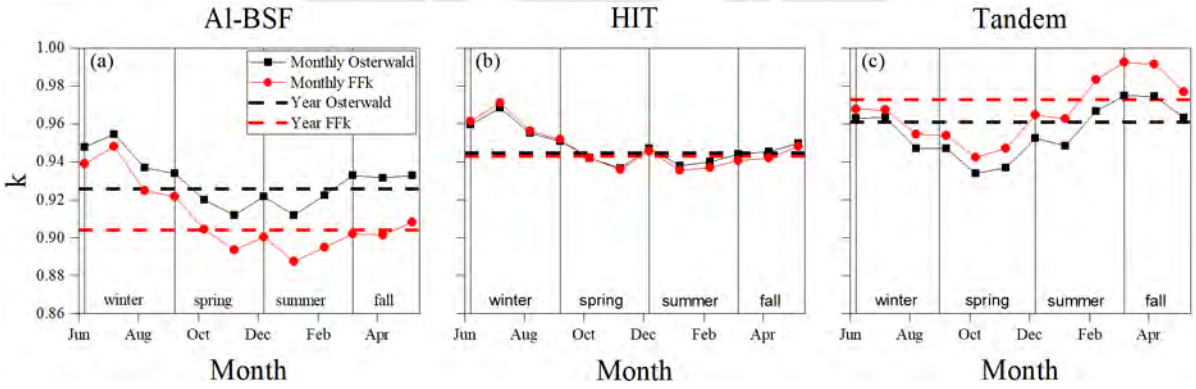

Figure 19. Correction Constant on a monthly and annual basis for both models and three technologies: (a) Al-BSF, (b) HIT, and (c) Tandem, from June 2019 to May 2020.

First, it should be noted that the power predicted by both models is overestimated, i.e., k < 1 (slope a > 1), for every technology and any month. Second, we can observe similar behavior for both models and three technologies, i.e., when the Osterwald model's results increase or decrease from one month to another, so does the one from the FF_K model (Figure 19). Such similarity is expected since both models share similar linear dependencies on the irradiance; see equations (2), (3), (4), and (5). However, the k-values of both models can differ depending on the month/season and the technology, i.e., the higher difference in the last months. For instance, for the Al-BSF technology, Osterwald's model results in a k higher than the FF_K model for any month, which means that its predicted power is closer to the experimental power produced by the module. For both models, during spring and summer, the k reaches a minimum value and a maximum value during winter. Interestingly, for the HIT technology, k and power estimation by both models are very similar throughout the year, with only slight differences during summer and fall. The FF_K model results in higher k values than Osterwald's in the Tandem technology, especially at the end of summer. Furthermore, for the Tandem technology, the seasonal behavior of k is different than for the other technologies. Here, the k-value reaches its highest value during summer/fall.

The distinct seasonal behavior of the different technologies indicates that irradiance and model temperature may not be sufficient to predict power correctly. Other parameters, which are not considered in the models, may also affect the estimated power depending on the season. These other parameters could be ambient parameters, such as the diffuse irradiance or the spectral distribution. The crystalline and thin-film silicon technologies may respond differently to these additional parameters due to the distinct low irradiance behavior, angular response, and spectral response [20]. Further measurements of another year are needed to corroborate if the observed seasonal trends of their k values are periodic.

Some trends of the monthly k values can also be observed in Figure 19. For Al-BSF technology, the annual k obtained from Osterwald's model is higher than that obtained from the FF_K model. While HIT technology presents k values are almost the same for both models. The Tandem technology works better with the FF_K model; its annual k values are the closest to 1 among the three technologies, meaning that the maximum power prediction of both models works most accurately for the Tandem PV technology.

6.2.2 Effective parameters

Figure 20 shows the values of the effective parameters, $P_M{}^*_{eff,}$ and FF^*_{eff}, which are calculated using k as shown in equations (15) and (16). Hence, they demonstrate the same behavior and trends observed for *k* in Figure 19. It should be noted that the superior limits of the y-axis in Figure 20 (a), (b), and (c) are the calibrated values from Table 2 as a reference to visualize the difference of the effective values to the calibrated ones nearest to STC. It can be drawn a similar conclusion for the effective parameters for k: each module's behavior could be attributed to the yearly average impact of other ambient parameters not considered in the models.

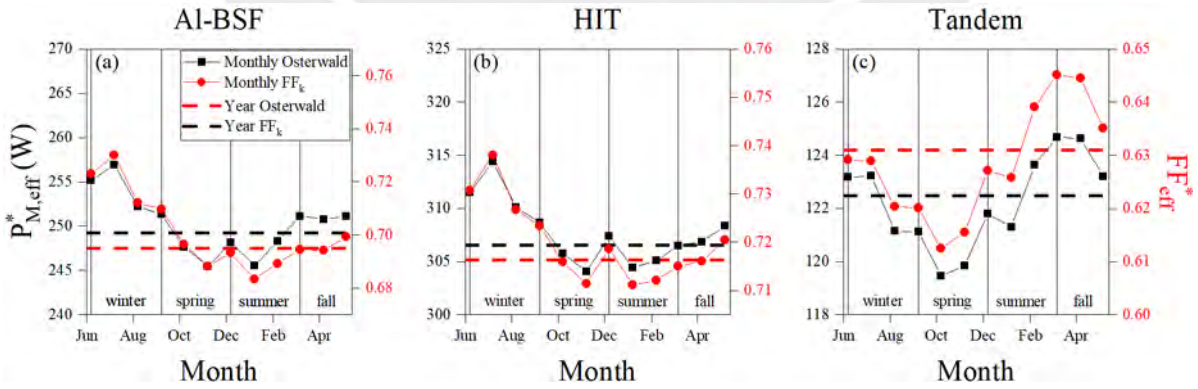

Figure 20. Effective parameters on a monthly and annual basis for both models and three technologies: (a) Al-BSF, (b) HIT, and (c) Tandem.

With the resulting effective parameters in Figure 20, we can recalculate the modeled power with Equations (2) and (3) each month and the entire year. After implementing the correction factor, the linear tendency was corroborated to analyze each method's quality. The

latter is observed in Figure 21, where the relation between the measured and the modeled power using the effective parameters for 1-year is equal to 1.

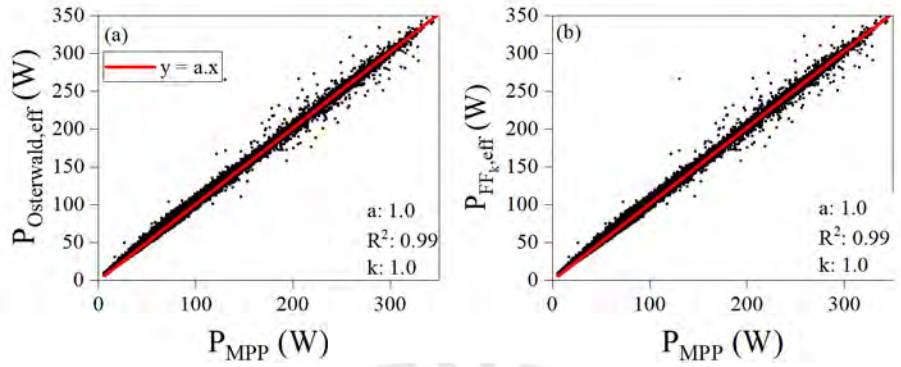

Figure 21. Correlation of the corrected modeled and measured power using (a) Osterwald's and (b) FF_k model. 1-year of data for the HIT solar cell module.

6.2.3 Error analysis

Figure 22 depicts each PV technology's resulting monthly and annual NRMSE values after implementing the correction factor. It is worth mentioning that a minimum of 2000 measurements was analyzed for each month for each technology. Hence, the NRMSE value is based on sufficient data sets to have a reliable statistic to re-construct the error distribution, as suggested in [65]. In Figure 22, both models result in very similar NRMSEs and dispersion for any month and technology. However, for all three technologies, one can observe that the monthly NRMSE value has a maximum in August and decreases from spring to fall. It will be interesting to see if this behavior is periodic and repeats itself in the following years. The Tandem technology shows the highest annual NRMSE value and the HIT the lowest. Further studies will aim at a better understanding of this behavior.

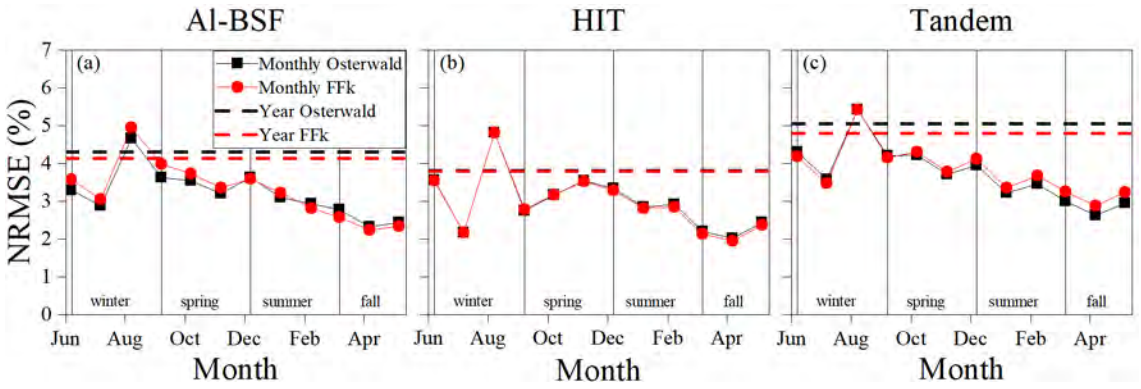

Figure 22. Normalized Root Mean Square Error (NRMSE) for each technology and model on a monthly and annual basis: (a) Al-BSF, (b) HIT, and (c) Tandem.

Figure 23 depicts the monthly and annual values of the NMBE for the three PV technologies. All NMBE values are relatively small, below 1%, which is expected since the purpose of implementing the correction factor was to minimize the NMBE. Nevertheless, a positive NMBE value indicates that the model is still overestimating; a negative value means it underestimates the power. In the Al-BSF case, for Osterwald's model, the annual NMBE is closest to 0, implying that the correction factor's implementation seems to be most effective for this technology in maximizing the prediction accuracy. The FF_K model tends to underestimate the power. Both models present similar annual, positive NMBE values for the HIT technology. These remain primarily stable during the entire year, slightly overestimating the modeled power with values ranging from 0 to 0.8 %. For the Tandem, both models tend to overestimate the measured power with a tendency to higher values over the months. Osterwald's method results in lower NMBE values than the FF_K method.

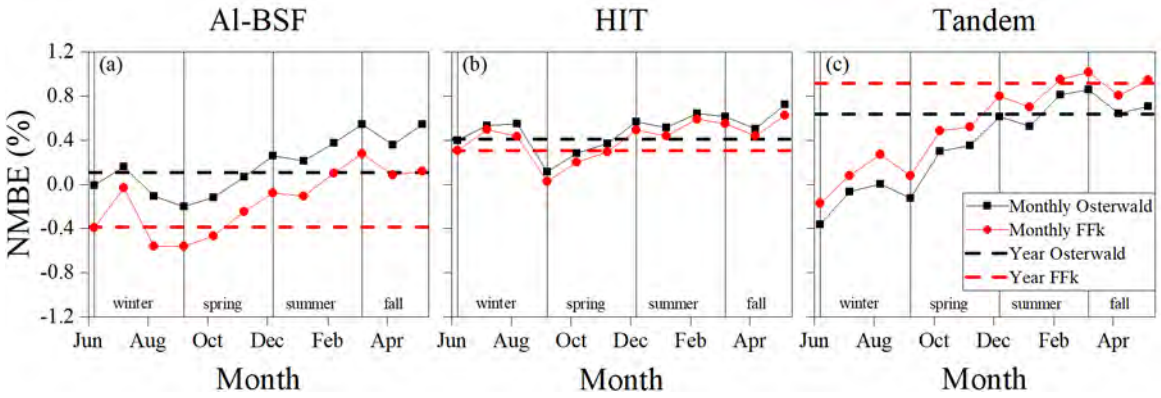

Figure 23. Normalized Mean Bias Error (NMBE) for each technology and model on a monthly and annual basis: (a) Al-BSF, (b) HIT, and (c) Tandem.

Table 5 summarizes the annual values of the calculated parameters k, $P^*_{M,eff}$, FF^*_{eff}, NRMSE, and NMBE, each for both models and three technologies. For the Al-BSF technology, the correction factor closer to 1 implies that Osterwald's model better predicts the power than the constant fill factor model when using the calibrated parameters, i.e., without the correction factor k. Furthermore, for the Osterwald model, lower absolute values of NRMSE and NMBE are closer to zero, implying that this is also the case after applying the correction factor and using the effective parameters for the power prediction. Whereas for the HIT technology, there is no apparent difference in using either model with or without k since their k values and NRMSE and NMBE are similar. Finally, the FF_K method may be recommended for the Tandem technology if calibrated values are used for power prediction due to its slightly lower k value. However, Osterwald's model behaves somewhat better if the correction factor is applied, as seen by the lower NRMSE and NMBE values.

Table 5. Annual values of k, effective parameters, NRMSE, and NMBE; for Osterwald and FF_k model for each technology (Al-BSF, HIT, and Tandem).

Technology	Method	k	$P^*_{M,eff}$ (W)	FF^*_{eff}	$NRMSE$ (%)	$NMBE$ (%)
Al-BSF	Osterwald	0.93	249.20	-	3.50	0.11
	FF_k	0.90	-	0.69	3.63	-0.39
HIT	Osterwald	0.94	306.52	-	3.10	0.40
	FF_k	0.94	-	0.72	3.08	0.28
Tandem	Osterwald	0.96	122.47	-	4.13	0.64
	FF_k	0.97	-	0.63	4.46	0.91

7 Conclusions and outlook

This work studied two different PV generators, one on PV plant level and another on PV module level. Therefore, the conclusion section is divided for each case. First, for half a year of monitoring a PV generator located in Granada, Spain. Alongside the procedure for estimating the nominal power where the hysteresis effect was present. A second comparison of the modeled and the measured power using two models for the first year of operation of three different PV module technologies installed in Lima, Peru.

7.1 Nominal power estimation of a PV generator

The procedure suggested by Martínez-Moreno [54] was applied to estimate the nominal power (P_M^*) of a 109.44 kW PV generator under working conditions for six months, from March to September 2018. A filtering procedure was implemented to filter the data from clear-sky days within the experimental period to achieve this. Nonetheless, these days demonstrated a difference in power before noon and in the afternoon, despite similar irradiance and temperature conditions, resulting in a hysteresis formation of the temperature-corrected power versus the irradiance. The hysteresis consisted of a linear part before noon and a non-linear part in the afternoon. The non-linear part datasets are assumed not to represent a PV generator's normal behavior, considering only the linear part for the P_M^* estimation results in a P_M^* of 104,24 kW with σ of 0.05. This additional step to the Martinez-Moreno methodology seemed appropriate to clarify the process to determine the P_M^* of a PV generator.

A possible cause for the hysteresis effect within the "Calerilla" PV generator could be either spatial or temporal inhomogeneities in the temperature and irradiance. More distributed equipment to measure module temperature and irradiance need to be installed to determine representative values to sections of the generator. The most likely source was spatial inhomogeneities of module temperature and plane-of-array irradiance due to misalignment of

the inclinations of strings. Such misalignments result in different angles of incidence between the irradiance measuring module and some PV strings, signaling the challenge of monitoring large PV generators. Similarly, the cell temperature measuring module cannot register possible inhomogeneities between the entire PV generator strings. Origins of the hysteresis and a more detailed explanation were published during the redaction of this thesis [64], where a new procedure to estimate the effective nominal power was proposed.

7.2 Modeling the power of three PV module technologies

During one year, the experimental campaign compared the measured power of three PV technologies, Al-BSF, HIT, and a-Si/µc-Si Tandem, with the modeled power using two relatively simple models: Osterwald's and Constant Fill Factor (FF_K). The experimental power was monitored through the maximum power point of I-V curve measurements. The models predicted the power based on measurements of the in-plane irradiance and the module temperature. Depending on the month and PV technology, both models overestimate the estimated power by about 2 to 10%. A correction factor (k) was introduced monthly and annually to minimize the overestimation. The monthly values of k indicated different trends during the different seasons of the year.

The seasonal trends for each PV technology are different, particularly when comparing the crystalline-based technologies, Al-BSF and HIT, with the a-Si/µc-Si Tandem thin-film technology. These trends could be associated with variables other than the irradiance and module temperature that the models do not consider, such as the spectral distribution or the diffuse irradiance factor [66]. A study similar to [20] is recommended to understand the impact of each variable on the seasonal trend.

By applying k to the models on an annual basis, the NMBE of the predicted maximum power was minimized for all technologies. NMBEs below 1% indicates a high accuracy in their

prediction capability. Furthermore, NRMSEs below 5% indicates a low predicted values dispersion. A closer look, seeking technology-specific evaluations of both models' prediction capabilities, suggests that: For the Al-BSF technology, Osterwald's model can be recommended for estimating the power in any case with or without the implementation of the correction factor. There is no apparent difference between the two models in their prediction accuracy, neither before nor after applying a correction factor for HIT technology. In the case of Tandem technology, the FF_K model is recommended when using the electrical calibration parameters, while Osterwald's model performs slightly better when implementing the correction factor. The measurements of one more year would be interesting to corroborate a similar seasonal behavior of the correction factor. Additionally, testing more analytical, iterative, and translation models [29] would be interesting to explore the performance of each one and recommend specific use for each technology.

8 Publications

Publications in the framework of this thesis:

B. Calsi, J. Angulo, L. Conde, E. Muñoz, R. Grieseler, J. Guerra, J. de la Casa, and J. Töfflinger: 'Procedure for calculating the nominal power of a photovoltaic generator', Tecnia, vol. 30 (2020).

B. Calsi, L. Conde, J. Angulo, J. Montes, J. Guerra, J. de la Casa, and J. Töfflinger: Monitoring versus prediction of the power of three different PV technologies in the coast of Lima-Peru', IOP Publishing, vol. 1841 (2021).

Other publications involving the author:

J. Angulo, B. Calsi, L. Conde, E. Muñoz, R. Grieseler, J. Guerra, J. de la Casa, and J. Töfflinger: 'Modeling of the nominal power of a PV generator under clear and cloudy sky conditions,' ISES Solar World Congress 2019.

J. Angulo, B. Calsi, E. Alfaro, L. Conde, E. Muñoz, R. Grieseler, J. Guerra, J. Töfflinger, R. Espinoza, and J. de la Casa: 'Study of the dust effect and the nominal power estimation in a photovoltaic string', Tecnia, vol.30 (2020).

L. Conde, J. Montes, A. Carhuavilca, R. Perich, J. Guerra, M. Sevillano, B. Calsi, J. Angulo, J. de la Casa, and J. Töfflinger: 'Implementation of a laboratory for the outdoor characterization of photovoltaic technologies under the climatic conditions of Lima,' Tecnia, vol. 30 (2020).

J. Angulo, B. Calsi, L. Conde, J. Guerra, E. Muñoz, J. de la Casa, and J. Töfflinger: 'Estimation of the effective nominal power of a photovoltaic generator under non-ideal operating conditions,' Solar Energy, vol.231 (2022).

Conferences participation:

B. Calsi, J. Angulo, L. Conde, E. Muñoz, R. Grieseler, J. Guerra, J. de la Casa, and J. Töfflinger: 'Procedure for calculating the nominal power of a photovoltaic generator', 21st November 2019, *Simposio peruano de energía solar* SPES 2019.

B. Calsi, L. Conde, J. Angulo, J. Montes, J. Guerra, J. de la Casa, and J. Töfflinger: 'Monitoring versus prediction of the power of three different PV technologies in the coast of Lima-Peru,' June 25th 2020, *Jornada Peruana de Energía Solar* JOPES 2020

9 Bibliography

[1] Smets A H, Jäger K, Isabella O, Swaaij van R A and Zeman M 2016 *Solar energy: the physics and engineering of photovoltaic conversion technologies and systems*

[2] Andre T 2020 *Renewables 2020 Global Status Report*

[3] Dr. P. Jayakumar 2009 *Asian and Pacific Centre for Transfer of Technology*

[4] Pandey A K, Tyagi V V., Selvaraj J A, Rahim N A and Tyagi S K 2016 Recent advances in solar photovoltaic systems for emerging trends and advanced applications *Renew. Sustain. Energy Rev.* **53** 859–84

[5] Fraunhofer Institute for Solar Energy Systems 2020 Photovoltaics Report *ise.fraunhofer.de/content/dam/ise/de/documents/publications/studies/Photovoltaics-Report.pdf*

[6] Solargis 2019 Photovoltaic Power Potential

[7] Mojonero D H, Villacorta A R and Kuong J L 2018 Impact assessment of net metering for residential photovoltaic distributed generation in Peru *Int. J. Renew. Energy Res.* **8** 1200–7

[8] Osinergmin 2019 *Energías Renovables: Experiencia y Perspectivas en la Ruta del Perú Hacia la Transición Energética*

[9] Osinergmin 2020 *Supervisión de Contratos de Proyectos de Generación y Transmisión de Energía Eléctrica en Operación*

[10] Osinergmin 2021 *Supervisión de Contratos de Proyectos de Generación y Transmisión de Energía Eléctrica*

[11] Jäger-Waldau A 2019 *PV Status Report 2019*

[12] Kelly G, Spooner T, Volberg G, Ball G and Bruckner J 2014 Ensuring the reliability of

PV systems through the selection of international standards for the IECRE conformity assessment system *2014 IEEE 40th Photovolt. Spec. Conf. PVSC 2014* 914–8

[13] International Electrotechnical Commission 2008 *Photovoltaic devices - Part 3: measurement principles for terrestrial photovoltaic (PV) solar devices with reference spectral irradiance data*

[14] Zaihidee F M, Mekhilef S, Seyedmahmoudian M and Horan B 2016 Dust as an unalterable deteriorative factor affecting PV panel's efficiency: Why and how *Renew. Sustain. Energy Rev.* **65** 1267–78

[15] García R, Torres-Ramírez M, Muñoz-Cerón E, de la Casa J and Aguilera J 2017 Spectral characterization of the solar resource of a sunny inland site for flat plate and concentrating PV systems *Renew. Energy* **101** 1169–79

[16] Mussard M and Amara M 2018 Performance of solar photovoltaic modules under arid climatic conditions: A review *Sol. Energy* **174** 409–21

[17] Afonso M M D, Carvalho P C M, Antunes F L M and Hiluy Filho J J 2015 Deterioration and performance evaluation of photovoltaic modules in a semi-arid climate *Renewable Energy and Power Quality Journal*

[18] Fouad M M, Shihata L A and Morgan E S I 2017 An integrated review of factors influencing the performance of photovoltaic panels *Renew. Sustain. Energy Rev.* **80** 1499–511

[19] Torres-Ramírez M, Nofuentes G, Silva J P, Silvestre S and Muñoz J V. 2014 Study on analytical modelling approaches to the performance of thin film PV modules in sunny inland climates *Energy* **73** 731–40

[20] Schweiger M, Herrmann W, Gerber A and Rau U 2017 Understanding the energy yield of photovoltaic modules in different climates by linear performance loss analysis of the

module performance ratio *IET Renew. Power Gener.* **11** 558–65

[21] Espinoza R, Luque C and Casa J De 2016 Missing gaps in the challenge of massive intervention of grid-connected PV systems in Peru *European Photovoltaic Solar Energy Conference and Exhibition* pp 3048–52

[22] Feron S and Cordero R R 2018 Is Peru prepared for large-scale sustainable rural electrification? *Sustain.* **10** 1–20

[23] Zambrano-Monserrate M A, Silva-Zambrano C A, Davalos-Penafiel J L, Zambrano-Monserrate A and Ruano M A 2018 Testing environmental Kuznets curve hypothesis in Peru: The role of renewable electricity, petroleum and dry natural gas *Renew. Sustain. Energy Rev.* **82** 4170–8

[24] MINEM 2018 Proyecto de Decreto Supremo que Aprueba el Reglamento de Generación Distribuida 8

[25] Ismodes F 2018 *Autorizan publicación de proyecto de Decreto Supremo que aprueba el Reglamento de la Generación Distribuida*

[26] Romero-Fiances I, Muñoz-Cerón E, Espinoza-Paredes R, Nofuentes G and de la Casa J 2019 Analysis of the Performance of Various PV Module Technologies in Peru *Energies* **12** 186

[27] Moser D, Del Buono M, Jahn U, Herz M, Richter M and De Brabandere K 2017 Identification of technical risks in the photovoltaic value chain and quantification of the economic impact *Prog. Photovoltaics Res. Appl.* **25** 592–604

[28] Osinergmin 2018 *Reporte de análisis económico sectorial sector electricidad Generación distribuida : marco normativo comparado para Perú , Chile , Colombia y México Año 6 – N ° 11 – diciembre 2018*

[29] Fuentes Conde M 2009 *Contribución al modelado del comportamiento eléctrico a sol real de módulos fotovoltaicos de silicio cristalino y CIS* (Universidad de Jaén)

[30] Conde L A, Montes-Romero J, Carhuavilca A, Perich R, Guerra J A, Sevillano M, Calsi B X, Angulo J R, De la Casa J and Töfflinger J A 2020 Implementation of a laboratory for the outdoor characterization of photovoltaic technologies under the climatic conditions of Lima *Tecnia* vol 30 pp 80–9

[31] Almonacid F, Rus C, Hontoria L, Fuentes M and Nofuentes G 2009 Characterisation of Si-crystalline PV modules by artificial neural networks *Renew. Energy* **34** 941–9

[32] Bottenberg W 1999 Module performance ratings: tutorial on history and industry needs *PV perfornmance, Realiability and Standars Workshop, NREL* pp 5–42

[33] Ferrada P, Marzo A, Cabrera E, Chu H, del Campo V, Rabanal J, Diaz-Almeida D, Schneider A and Kopecek R 2017 Potential for photogenerated current for silicon based photovoltaic modules in the Atacama Desert *Sol. Energy* **144** 580–93

[34] Osterwald C R 1986 Translation of device performance measurements to reference conditions *Sol. Cells* **18** 269–79

[35] Meral M E and Diner F 2011 A review of the factors affecting operation and efficiency of photovoltaic based electricity generation systems *Renew. Sustain. Energy Rev.* **15** 2176–84

[36] Moharram K A, Abd-Elhady M S, Kandil H A and El-Sherif H 2013 Enhancing the performance of photovoltaic panels by water cooling *Ain Shams Eng. J.* **4** 869–77

[37] Rodrigues E and Melicio R 2011 Simulation of a Solar Cell considering Single-Diode Equivalent Circuit Model Simulation of a Solar Cell considering Single-Diode Equivalent Circuit Model Key words *International Conference on Renewable Energies and Power Quality*

[38] Segado P M 2015 *Contribución al estudio de la temperatura de módulos FV de diferentes tecnologías en condiciones de sol real* (Universidad de Málaga)

[39] Lorenzo E 2006 *Radiación solar y dispositivos fotovoltaicos, Volumen ll. Electricidad solar fotovoltaica*

[40] Luque A and Hegedus S 2003 *Handbook of photovoltaic science and engineering*

[41] Gholami A, Saboonchi A and Alemrajabi A A 2017 Experimental study of factors affecting dust accumulation and their effects on the transmission coefficient of glass for solar applications *Renew. Energy* **112** 466–73

[42] El-Shobokshy M S and Hussein F M 1993 Degradation of photovoltaic cell performance due to dust deposition on to its surface *Renew. Energy* **3** 585–90

[43] Reiß S, Grieseler R, Krischok S and Rädlein E 2018 The influence of Sahara sand on the degradation behavior of float glass surfaces *J. Non. Cryst. Solids* **479** 16–28

[44] Lamont L A and El Chaar L 2011 Enhancement of a stand-alone photovoltaic system's performance: Reduction of soft and hard shading *Renew. Energy* **36** 1306–10

[45] Hermann W, Becker H and Wiesner W 1997 Round robin test on translation procedures for measured PV generator charasteristic *Proceedings of tht 14th Photovoltaic Solar Energy Conference, Barcelona* pp 203–6

[46] Rus-Casas C, Aguilar J D, Rodrigo P, Almonacid F and Pérez-Higueras P J 2014 Classification of methods for annual energy harvesting calculations of photovoltaic generators *Energy Convers. Manag.* **78** 527–36

[47] Fuentes M, Nofuentes G, Aguilera J, Talavera D L and Castro M 2007 Application and validation of algebraic methods to predict the behaviour of crystalline silicon PV modules in Mediterranean climates *Sol. Energy* **81** 1396–408

[48] Filik U B, Filik T and Gerek O N 2018 A hysteresis model for fixed and sun tracking solar PV power generation systems *Energies* **11** 603

[49] Huld T, Müller R and Gambardella A 2012 A new solar radiation database for estimating PV performance in Europe and Africa *Sol. Energy* **86** 1803–15

[50] Muñoz-Cerón E, Lomas J C, Aguilera J and de la Casa J 2018 Influence of Operation and Maintenance expenditures in the feasibility of photovoltaic projects: The case of a tracking pv plant in Spain *Energy Policy* **121** 506–18

[51] Martínez-Moreno F 2012 *Caracterización y modelado de grandes centrales fotovoltaicas*

[52] Moretón Villagrá R 2016 *Contributions to uncertainty reduction in the estimation of PV plants performance*

[53] Lomas Monzón J C 2019 *Retrospectiva técnica y de modelo de negocio de los sistemas fotovoltaicos conectados a la red en España*

[54] Martínez-Moreno F., Lorenzo E., Muñoz J. M R 2012 On the testing of large PV arrays *Prog. Photovoltaics Res. Appl.* **20** 100–5

[55] Conde L A, Montes-Romero J, Carhuavilca A, Perich R, Jorge A, Angulo J, Muñoz E, Töfflinger J A and Casa J De 2020 Performance evaluation and characterization of different photovoltaic technologies under the coastal , desertic climate conditions of Lima , Peru *Solar World Congress* p 11

[56] Montes-Romero J, Piliougine M, Muñoz J V, Fernández E F and De La Casa J 2017 Photovoltaic device performance evaluation using an open-hardware system and standard calibrated laboratory instruments *Energies* **10** 1869

[57] Ishii T, Otani K and Takashima T 2011 Effects of solar spectrum and module

temperature on outdoor performance of photovoltaic modules in round-robin measurements in Japan *Prog. Photovoltaics Res. Appl.* **19** 141–8

[58] Dunn L, Gostein M and Emery K 2012 Comparison of pyranometers vs. PV reference cells for evaluation of PV array performance *Conf. Rec. IEEE Photovolt. Spec. Conf.* 2899–904

[59] Reynolds S and Smimov V 2012 Modelling of two-and four-terminal thin-film silicon tandem solar cells Modelling of two-and four-terminal thin-film silicon tandem solar cells *J. Phys. Conf. Ser.* **398** 012006

[60] Silva J S, Rojas J P, Norabuena M and Seguel R J 2018 Ozone and volatile organic compounds in the metropolitan area of Lima-Callao, Peru *Air Qual. Atmos. Heal.* **11** 993–1008

[61] International Electrotechnical Commission 2008 International Standard *60751* 41

[62] International Electrotechnical Commission 2008 International Standard *61298-1* 34

[63] Ramon Ruiz G and Fernández Bandera C 2017 Validation of Calibrated Energy Models: Common Errors *Energies* **10** 1587

[64] Angulo J R, Calsi B X, Conde L A, Guerra J A, Muñoz-Cerón E, de la Casa J and Töfflinger J A 2021 *Estimation of the effective nominal power of a photovoltaic generator under non-ideal operating conditions*

[65] Chai T and Draxler R R 2014 Root mean square error (RMSE) or mean absolute error (MAE)? - Arguments against avoiding RMSE in the literature *Geosci. Model Dev.* **7** 1247–50

[66] Conde L A, Angulo J R, Sevillano-Bendezú M, Nofuentes G, Töfflinger J A and de la Casa J 2021 Spectral effects on the energy yield of various photovoltaic technologies in

Lima (Peru) *Energy* **223**